Available online at www.sciencedirect.com
ScienceDirect
Journal of Asian Earth Sciences 30 (2007) 423–432
Journal of Asian Earth Sciences
www.elsevier.com/locate/jaes

Fine-tuning of age integrating magnetostratigraphy, radiocarbon dating, and carbonate cyclicity: Example of lacustrine sediments from Heqing basin (Yunnan, China) covering the past 1 Myr

Shouyun Hu [a,d], Srinivasa Rao Goddu [b], Erwin Appel [b,*], Ken Verosub [c]

[a] Nanjing Institute of Geography and Limnology, Chinese Academy of Sciences, 73 East Beijing Rd, Nanjing 210008, China
[b] Institut für Geowissenschaften, Universität Tübingen, Sigwartstr. 10, 72076 Tübingen, Germany
[c] Department of Geology, University of California, Davis, CA 95616, USA
[d] Department of Geography, Shanghai Normal University, Shanghai 200234, China

Received 27 June 2005; received in revised form 19 October 2006; accepted 14 November 2006

Abstract

High-resolution magnetostratigraphy, wavelength spectra of carbonate cyclicities, and AMS radiocarbon dating are integrated to establish an optimum age model for a 168 m long drill core of lacustrine sediments from Heqing basin, Yunnan Province, southwestern China. A ^{14}C age of 51.62 +2.42/−1.85 kyr BP is obtained at a depth of 7.3 m. Remanent magnetization is carried by maghemite and partly in addition by magnetite, both showing the same direction. The polarity sequence clearly reveals the Brunhes/Matuyama (B/M) boundary at 141.5 m. Blake Event is found between 16.3 and 17.5 m, and the upper boundary of Jaramillo is indicated at 167.0 m. Carbonate content and magnetic susceptibility were used for spectral analysis. Fourier analysis was done on the depth section for sliding windows with different window lengths. The spectra within the range of window centers (30–140 m) show a dominant long wavelength, which changes from about 18.5 m in the lower part (>65 m depth) to about 14.5 m in the upper part (<65 m depth) of the core. It is assumed that the long wavelength peak represents the 95-kyr Milankovitch eccentricity cycle. The B/M boundary and Blake Event match very well with this model, but the age of Jaramillo is strongly underestimated. Fourier spectra of sliding windows slightly indicate a drop of the sedimentation rate at the lowermost part of the core. An *optimum age model* is calculated by cubic spline interpolation using tie points from ^{14}C dating, magnetostratigraphy ('true' ages of Blake Event, B/M boundary, and Jaramillo), and wavelengths of carbonate (change in sedimentation rate at 65 m). Alternative depth-to-age transfer functions were tested, i.e. a wavelength age model (using sedimentation rates with ^{14}C as a tie point), a cyclostratigraphic model (using bandpass-filtered carbonate data corresponding to 95 kyr eccentricity cycles) and correlation of carbonate variations to the marine oxygen isotope curve. However, none of the approaches lead to a convincing Milankovitch spectrum of whole-core carbonate data. The Fourier spectra of whole-core carbonate and susceptibility time series calibrated by the optimum age model show clear Milankovitch cyclicities (95, 41, 23, and 19 kyr) indicating that a global palaeoclimatic signal is recorded. According to this result the Heqing core spans almost the complete past 1 Myr (5–1001 ka). Detailed depth-to-age conversion is listed. The optimum age model can be used as a fine-tuned time basis for interpreting the existing data set of palaeoclimatic proxies which have been already measured for this sequence.
© 2007 Elsevier Ltd. All rights reserved.

Keywords: Magnetostratigraphy; Lacustrine sediments; Orbital tuning; Milankovitch cyclicities; Spectral analysis

1. Introduction

Lacustrine sediments are a suitable archive for records of palaeoenvironmental changes on different time scales

* Corresponding author. Tel.: +49 (0)7071 2974132; fax: +49 (0)7071 295820.
E-mail address: erwin.appel@uni-tuebingen.de (E. Appel).

1367-9120/$ - see front matter © 2007 Elsevier Ltd. All rights reserved.
doi:10.1016/j.jseaes.2006.11.007

(Thouveny et al., 1994; Williams et al., 1997; Wang et al., 1999). A reliable and accurate age frame is a fundamental requirement for any such interpretation. Radiocarbon dating provides a powerful tool for periods younger than about 60 ka. Beyond the range of ^{14}C lifetime absolute dating methods are very limited and their applicability is restricted to favourable cases. Magnetostratigraphy has been particularly successful for long lacustrine sequences (Williams et al., 1997; Burbank and Johnson, 1982). Linear interpolation between reversals can be applied to establish a first-order age model supposed that the rate of sedimentation is rather constant throughout the sequence. However, lacustrine sedimentation with a constant rate of deposition rarely exists through longer periods. For obtaining a better resolution cyclostratigraphy can be employed (Schwarzacher, 1993; House, 1985; Ruddiman et al., 1986). The linkage between climate and Milankovitch cycles, i.e. the Earth's orbital eccentricity (present-day periods of 413 and 95 kyr), obliquity (41 kyr) and precession of equinoxes (23 and 19 kyr), has been recognized since long time in marine sediments (Ruddiman et al., 1986; Kukla et al., 1988). Significant evidence was also obtained from long continental records as loess-palaeosol sequences of Quaternary age (Kukla et al., 1988; Kukla and Clerk, 1996) and even Cretaceous sediments (Herbert, 1992; Mayer and Appel, 1999). To our knowledge no such approach has been reported from lacustrine sections.

In this paper, we present a study on a 168 m long core of lacustrine sediments from the central part of Heqing basin, Yunnan Province, China. The record of magnetic parameters, carbonate, pollen and spores, total organic carbon, and grain size distribution was interpreted by in terms of palaeoclimatic variations. The carbonate is most likely of detrital origin (Hu et al., 2005). Pollen data indicate alternations between temperate-arid and cold-humid conditions (Yang et al., 2000; Hu et al., 2005). Highs (maghemite and magnetite) and lows (maghemite only) of magnetic susceptibility was related to warm and cold periods, respectively (Hu et al., 2005). Magnetic and non-magnetic data show a clear change at 65 m (corresponding to ~410 ka) indicating a change in the depositional system related to a climatic and/or tectonic event (Hu et al., 2005).

It is assumed that the sequence covers a major part of the Quaternary. Our aim is to determine an optimum age model for the Heqing core. We suggest a new method by combining discrete time markers derived from magnetostratigraphy, radiocarbon dating, and cyclic sedimentation.

2. Samples

Heqing basin (100°06′–100°29′E, 25°51′–26°46′N) is situated in northwestern Heqing County, Yunnan Province, China, at the southeastern fringe of the Tibetan plateau (Fig. 1). It is surrounded by mainly limestones and granites, which are expected to be the main detrital source.

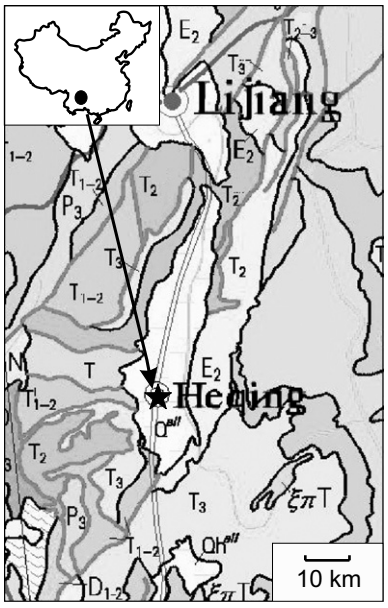


Fig. 1. Location of Heqing basin and geological map of the basin and its surrounding. The star in the center of the basin shows the position of the Heqing core. Q: Quaternary basin, N: Neogene, E: Paleogene, T: Triassic, P: Permian, D: Devonian (mainly limestones); $\varepsilon\pi$T: Triassic intrusive rocks.

The basin fill sediments have a thickness of about 700 m (unpublished data from exploration industry). A 168 m long continuous drill core was recovered from the central part of the ancient lake. The sediments are essentially composed of mud throughout the whole core, they are not varved, but changes in colour are obvious. The detailed sedimentary description is as follows:

168–135 m: greenish grey, blue-grey and grey mud;
135–78 m: brown, grey and greenish grey mud;
78–11.6 m: green, greenish grey and dark grey mud;
11.6–4.0 m: yellow silty mud;
4.0–0.68 m: blue-grey mud with carbon particles;
0.68–0.15 m: yellow silty mud;
Above 0.15 m: agricultural cultivated soil.

A total of 1656 samples (mean sampling interval about 10 cm) were collected for palaeomagnetic and rock magnetic studies using cubic plastic boxes ($2 \times 2 \times 2$ cm). The samples were dried in air at room temperature prior to any magnetic measurements. Additionally 1096 samples were taken for carbonate analysis. Two suitable samples from the topmost part of the core were selected for radiocarbon dating.

3. Results

3.1. Radiocarbon dating

AMS ^{14}C dating was performed at the Leibniz Laboratory of Kiel University (Germany) on organic matter rich

samples from depths of 7.3 and 13.0 m. The sample from 7.3 m yields an age of 51.62 +2.42/−1.85 kyr BP, whereas for the older sample the lifetime of ^{14}C is exceeded.

3.2. Magnetic results

Magnetic parameters (susceptibility and laboratory remanences) have been measured all along the core for palaeoenvironmental interpretation (Hu et al., 2005). In this paper we present magnetic results which are important for polarity stratigraphy. Susceptibility variations, measured by a Bartington MS2B instrument, are used for spectral analysis.

3.2.1. Demagnetization behaviour

Pilot samples were chosen for stepwise alternating field (AF) demagnetization (98 samples) and thermal demagnetization (90 samples) based on criteria of lithology and colour. Remanence measurements were made with a 2G SQUID magnetometer. AF demagnetization was carried out in a 2G degausser attached to the magnetometer, while for thermal demagnetization a MMTD18 furnace was used. All magnetic measurements were conducted in

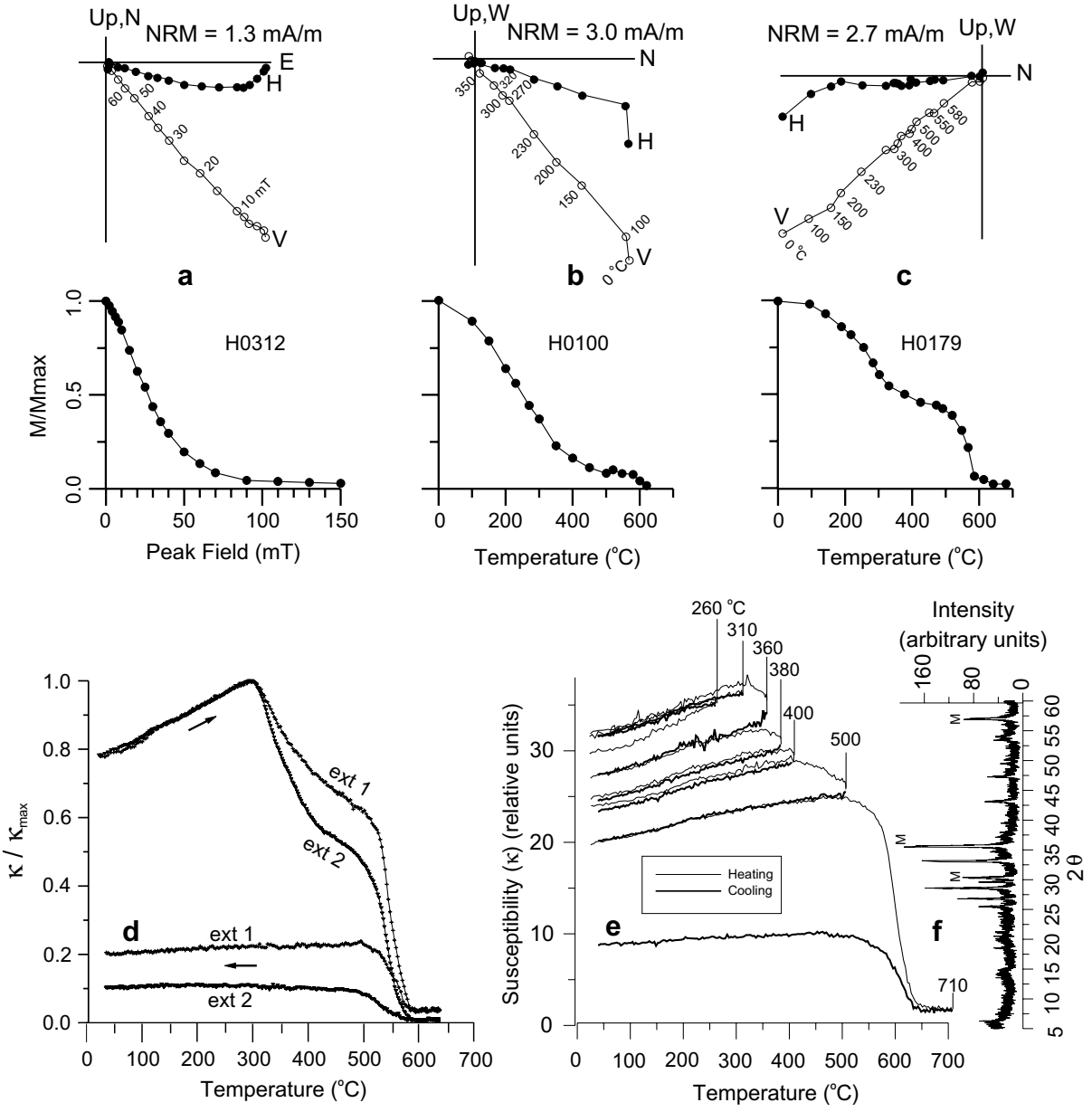


Fig. 2. Demagnetization behaviour of representative samples. (a) Stepwise AF demagnetization showing a predominance of soft remanence components. (b,c) Stepwise thermal demagnetization of representative samples with only LTC (b) and LTC+HTC (c). (d) Thermo-magnetic susceptibility runs on magnetic extracts; arrows represent heating and cooling curves. (e) Partial thermo-magnetic runs of a magnetic extract with successive heating steps; maximum temperatures are mentioned at their respective curves; breakdown of the LTC (maghemite) starts from ca. 320 °C. (f) X-ray diffraction analysis showing the presence of magnetite among other non-magnetic minerals. M represents magnetite.

the palaeomagnetic laboratory at Tübingen University. During AF demagnetization, the intensity was reduced to less than 10% by a field of 60 mT. Median destructive fields (MDFs) of about 25 mT indicate relatively soft magnetic minerals. After removal of a soft component at around 10 mT, the demagnetization paths generally show a univectorial behaviour pointing towards the origin (Fig. 2a).

Thermal demagnetization reveals two types of behaviour. In the first type, remanence intensity decreases mainly between 100 and 400 °C (Fig. 2b). In the following we call this component as the low temperature component (LTC). In the second type, another component (HTC) with higher unblocking temperatures close to the Curie temperature of magnetite (about 580 °C) appears in addition to the LTC (Fig. 2c). Samples with LTC and HTC tend to have a higher susceptibility than samples with a LTC only. It seems that HTC occurs additionally in some parts of the sequence (Fig. 3a).

The LTC and HTC show almost the same characteristic remanent magnetization (ChRM) directions. This indicates that both magnetic minerals were deposited or authigenically formed at (nearly) the same time. For the pilot samples, remanence components after AF cleaning of the soft component and after heating above 200 °C show similar ChRM directions. Since AF demagnetization is less time-consuming, and more suitable for fragile samples, it was used for the bulk of samples.

3.2.2. Magnetic mineral analysis

Thermo-magnetic runs of susceptibility (χ) were performed to determine magnetic mineralogy (using a CS-3 heating device attached to a KLY-3 susceptibility bridge). More than 40 samples of raw material, distributed along the whole core, were investigated. However, almost all curves show a strong intensity increase above ~350 °C due to secondary formation of magnetite masking the original magnetic mineralogy. Additionally, two magnetic extracts were prepared from depths of 21.69 and 28.44 m (ext1) and 135.35 and 146.44 m (ext2), both representing sediments with higher susceptibility. Both extracts show a similar behaviour (Fig. 2d). During heating, χ increases steadily towards a peak at about 300 °C. At higher temperatures, a decrease is observed at the

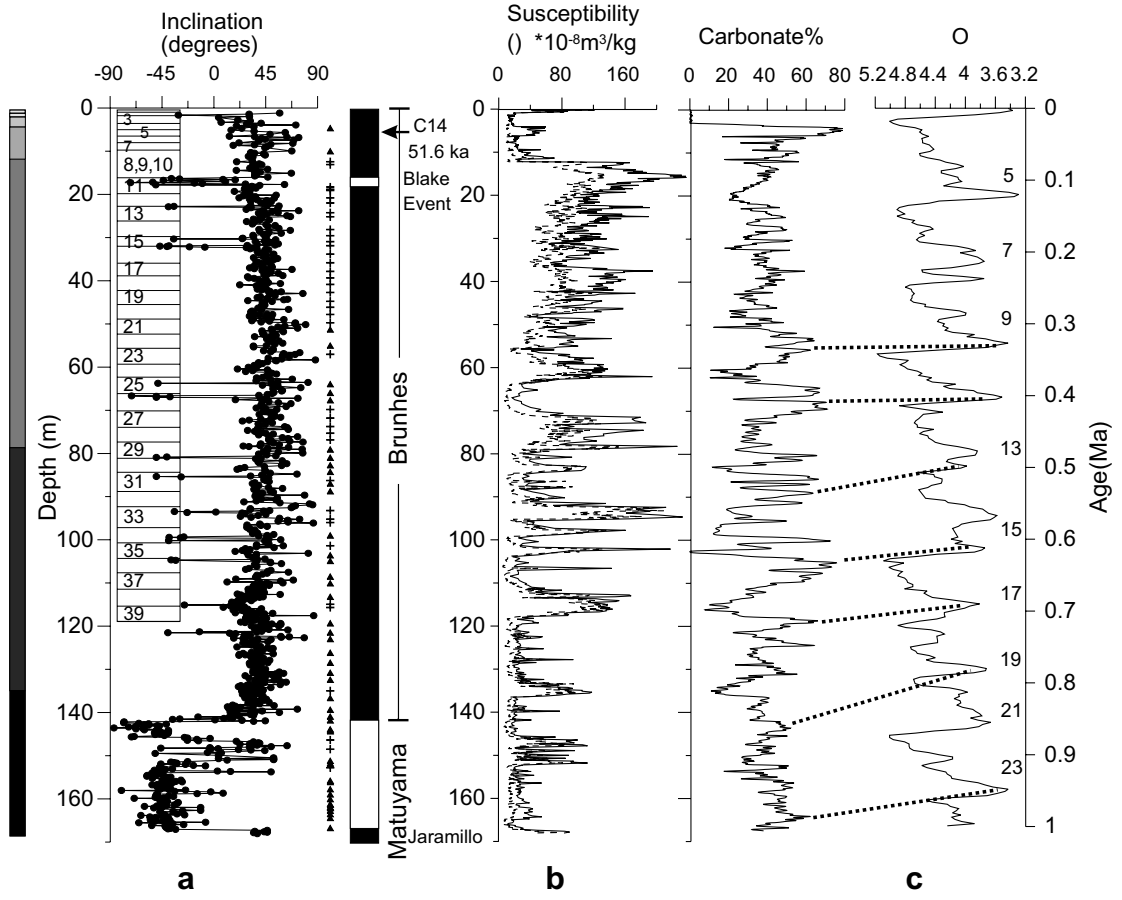


Fig. 3. (a) Results of magnetostratigraphy (inclination) with interpreted polarity sequence. Position of the sample giving a radiocarbon age is marked. Samples analysed in more detail for magnetic mineralogy are indicated: (△: LTC/maghemite only; +: LTC/maghemite and HTC/magnetite). Drilling turns (above 120 m) are plotted next to the depth scale. Lithology is shown at the left side; for explanation see text. (b) Magnetic susceptibility (smoothed by 5-point running average); the full line represents the carbonate corrected susceptibility. (c) Carbonate content (smoothed by 5-point running average) and its tentative correlation with marine oxygen isotope curve.

Curie temperature of magnetite (the carrier of the HTC). A second phase is indicated by deflection of the curves at around 400 °C (probably the carrier of the LTC). Cooling curves show only evidence for magnetite. Non-reversibility indicates that the second phase has been destroyed during heating. This let us assume maghemite or greigite to be responsible for the LTC. Two more magnetic extracts were prepared from depths of 21 and 92.2 m for partial thermo-magnetic runs. Both samples revealed a similar behaviour (Fig. 2e). No major mineral magnetic changes occur up to a temperature of 310 °C; the slight increase after first heating is likely related to stress release by annealing. After subsequent heating the LTC phase is gradually destroyed from ~320 to ~500 °C and probably converted to hematite which is a typical behaviour of maghemite. Greigite can be ruled out because it has a Curie temperature of around 300 °C and is usually destroyed below 300 °C (Hoffmann, 1992).

Part of magnetic extracts ext1 and ext2 were used for X-ray diffraction. Only magnetite could be identified (Fig. 2f); the second phase (maghemite) is probably below the detection limit of 5%.

3.2.3. Magnetic polarities

Magnetostratigraphy is based on magnetic inclinations only. Azimuthal orientation of the core could not be obtained. Declinations within individual parts are non-significant as drill cores were cut into short pieces of a few 10 cm length for transportation. Reconstruction of orientation by anisotropy of susceptibility failed because the samples show a typical sedimentary pattern (equal distribution of χ_{max} axes in the bedding plane).

Magnetic inclination versus depth is plotted in Fig. 3a. The Brunhes Chron is clearly indicated by predominantly positive inclinations down to 141.5 m depth. Some negative inclinations are observed within the Brunhes Chron. At depths of 16.3–17.5, 31.9–32.2, 66.7–67.0, and 99.3–99.5 m, there are at least three consecutive samples with negative inclinations. It is difficult to decide whether or not these may represent geomagnetic excursions during the Brunhes Chron. Many such negative inclinations are located at either the top or the bottom of drilling turns (Fig. 3a) and therefore could be artifacts caused by the drilling process.

However, one possible excursion may exist between 16.3 and 17.5 m defined by 11 consecutive samples (8 with negative and 3 with shallow positive inclinations). Although this part is close to the top of turn 11, it seems to be unlikely that so many samples are affected by the drilling process. Interpolation of the ^{14}C age and B/M boundary indicates that this represents a record of the Blake Event.

Another possible excursion may exist between 31.9 and 32.2 m defined with five consecutive samples. Based on Blake Event (~115 ka) and B/M boundary (780 ka) at around 17.5 and 141.5 m, respectively, the interpolated age for this possible excursion should be around 188 ka. This age is similar to the one reported for the Iceland Basin Event at around 190 ka (Channell and Raymo, 2003). However, these samples with negative inclinations are located directly at the bottom of a drilling turn, thus disturbance by the drilling process cannot be ruled out.

In the upper Matuyama Chron, at 146–151 m, samples with positive and intermediate inclinations frequently appear. It may appear like a record of Santa Rosa Event (Singer and Brown, 2002; Yang et al., 2004). However, this part is related to high susceptibility values and artifacts of the recording process may hide the record of the geomagnetic field behaviour (Verosub and Banerjee, 1977; Hu et al., 1998).

At the bottom of the core, eight consecutive samples show positive inclinations. The number of samples supports our view that they are not affected by drilling disturbances. We infer that this bottommost part could represent the top of the Jaramillo subchron.

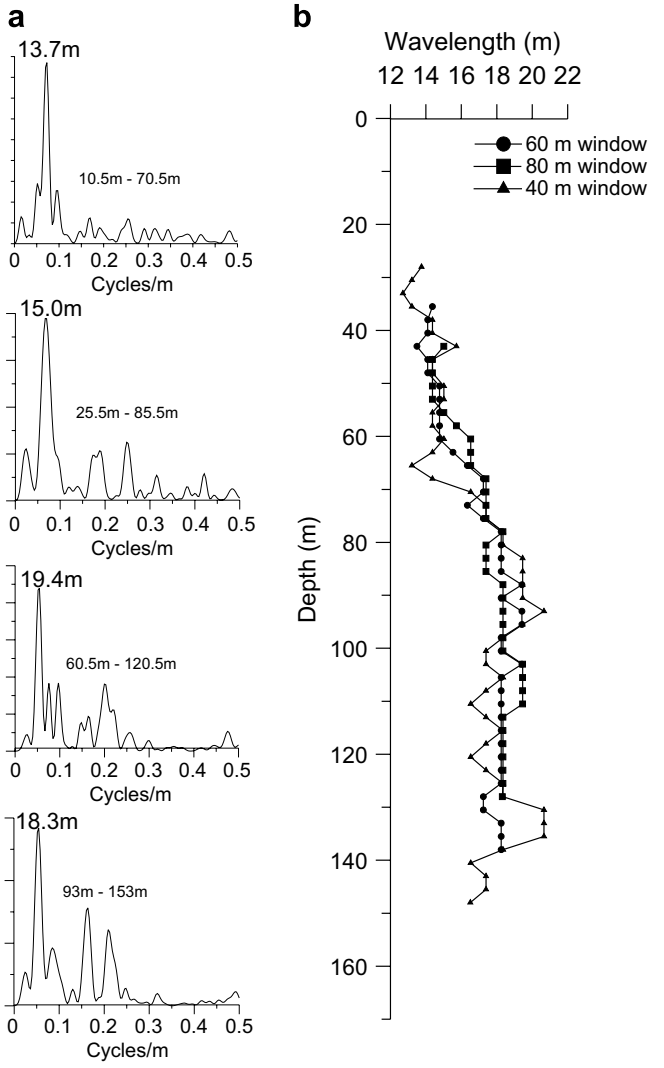


Fig. 4. Results from spectral analysis of carbonate in the wavelength domain. (a) Examples of spectra from sliding windows with different window lengths. (b) Wavelengths of the dominant spectral peak plotted versus depth at the center of their respective windows.

3.3. Wavelength analysis

Wavelength analysis (Fourier transformation) was performed on smoothed five-point running average carbonate data (Fig. 3c) for sliding windows with different window lengths of 40, 60, and 80 m (sliding intervals 2.5 m). The time series analysis toolbox of the STATISTICA software has been used.

For all spectra maximum power is found in the peak representing the maximum wavelength (Fig. 4a). As the core spans about 1 Myr (based on the ^{14}C age and B/M boundary) it is likely that this wavelength represents eccentricity. The wavelengths of these peaks obtained from sliding windows are plotted at the center of their windows along the depth (Fig. 4b). Results show a change in wavelengths between depths of 55 and 75 m indicating different sedimentological conditions below and above about 65 m. Changes in the pattern of carbonate and susceptibility variations (Fig. 3b and c) can also be seen at these depths (cyclicity is more obvious below 65 m). For shorter sliding windows the transition interval becomes shorter; the gradual shift of wavelengths between 55 and 75 m is obviously a smearing effect caused by the window length. With the assumption that wavelengths are constant above 65 m (14.5 m wavelength) and below 65 m (18.5 m wavelength) we can derive a discrete change for the rate of deposition from 15 cm/kyr (above 65 m) to 19 cm/kyr (below 65 m). However, it has to be noted that at 120–140 m a decrease of wavelengths is also indicated.

4. Discussion and optimum age model

In the following we test several methods to establish an age frame for the Heqing core. Spectral features of carbonate variations from the whole-core (after depth-to-time conversion) are checked for Milankovitch cyclicities to evaluate the reliability of our age calibration. The REDFIT software (Schulz and Mudelsee, 2002), which deals with unevenly spaced time intervals (including the same functions as the SPECTRUM software of Schulz and Stattegger, 1997), was used for spectral analysis of the complete core.

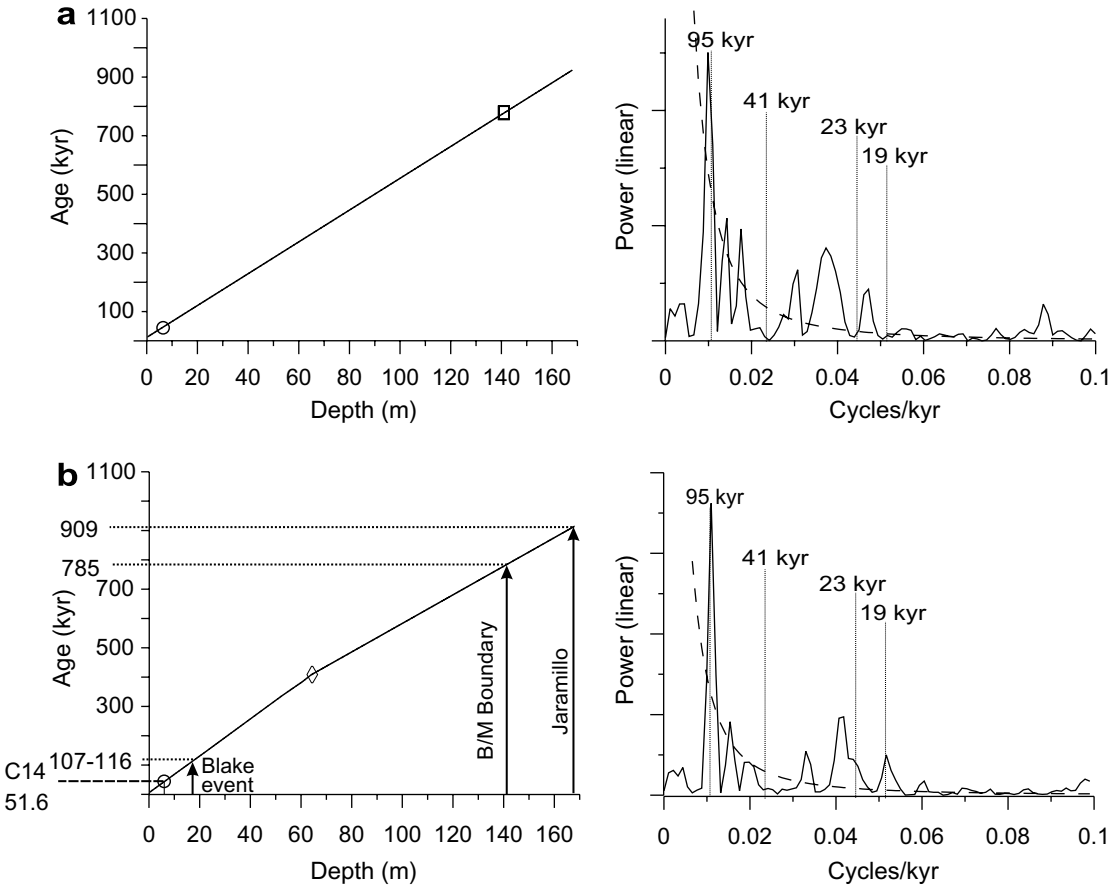


Fig. 5. (a) *Linear age model* using ^{14}C date at 7.3 m (51.6 ka; circle) and B/M boundary at 142.0 m (780 ka; square) as tie points, and corresponding Fourier spectrum of whole-core carbonate including significance level (dashed line). (b) *Wavelength age model* using sedimentation rates of 15 cm/kyr and 19 cm/kyr above and below 65 m (diamond) with ^{14}C age (circle) as a tie point. Results from magnetostratigraphy (reversals) are compared to this model: ages derived for Blake Event, B/M boundary, and upper Jaramillo boundary are given. The corresponding Fourier spectrum of whole-core carbonate is shown at the right side including significance level (dashed line).

The simplest approach is to determine a *linear age model* by using the most reliable tie points, B/M boundary and the ^{14}C date. The corresponding Fourier spectrum of carbonate of the complete section (Fig. 5a) shows the 95-kyr eccentricity peak, but precession peaks are shifted and there is no indication for obliquity.

A *wavelength age model* is obtained by using ^{14}C as a tie point and rates of deposition derived from wavelength analysis (15 cm/kyr for 0–65 m, 19 cm/kyr for 65–168 m). The obtained ages from the model are compared to the results of magnetostratigraphy. Ages derived from this model for Blake Event (116–107 ka) and B/M boundary (785 ka) match very well to the expected ages of ca. 115 ka (Bleil and Gard, 1989) and 780 ka (Cande and Kent, 1995), respectively (Fig. 5b), however, for the upper Jaramillo boundary (909 ka) there is a clear underestimation of the expected age (990 ka, Cande and Kent, 1995). This may be explained by a significantly lower sedimentation rate during the Matuyama Chron. As mentioned in Section 3.3 wavelengths of sliding windows versus depth reveal a tendency towards shorter wavelengths at their lowermost end (Fig. 4b). From Fig. 5b it is evident that the whole-core spectrum of carbonate of the wavelength age model shows no substantial improvement compared to the linear age model.

In another approach we use filtered curves of carbonate. As discussed above, Fourier analysis reveal wavelengths between 13 and 20 m for the eccentricity cycle. To resolve the eccentricity cycle along the core, a bandpass filter with low and high cutoff of 11 and 25 m was chosen (Fig. 6a). Bandpass filtering was done using the REFLEX software (Sandmeier Scientific Software). Taking ^{14}C age as a tie point and assuming that the time between consecutive peaks of the filtered curve is 95 kyr, the ages of the peaks were determined versus depth. The age of first peak (at 8.5 m) of the filtered

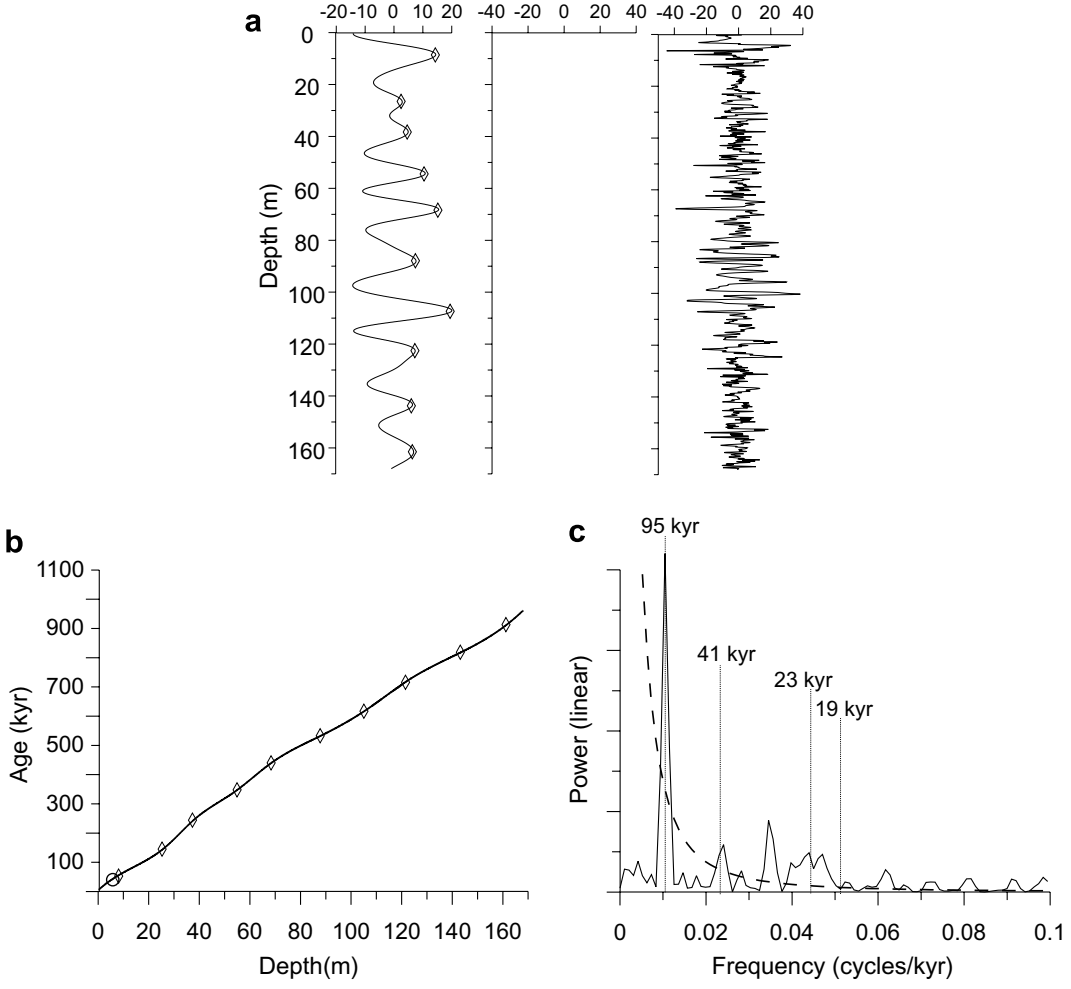


Fig. 6. Bandpass filtered curves of carbonate (cutoff of bandpass filters: eccentricity 25–11 m, obliquity 11–5 m, precession 5–1 m); corresponding ages of peaks are calculated based on the ^{14}C date at 7.3 m (51.6 ka). (b) *Bandpass age model*; used tie points for interpolation are shown (circle: ^{14}C; diamonds: deduced from bandpass filtered curve as in (a)). (c) Spectra of whole-core carbonate using the bandpass age model for both cubic spline interpolation; significance level is shown by dashed line.

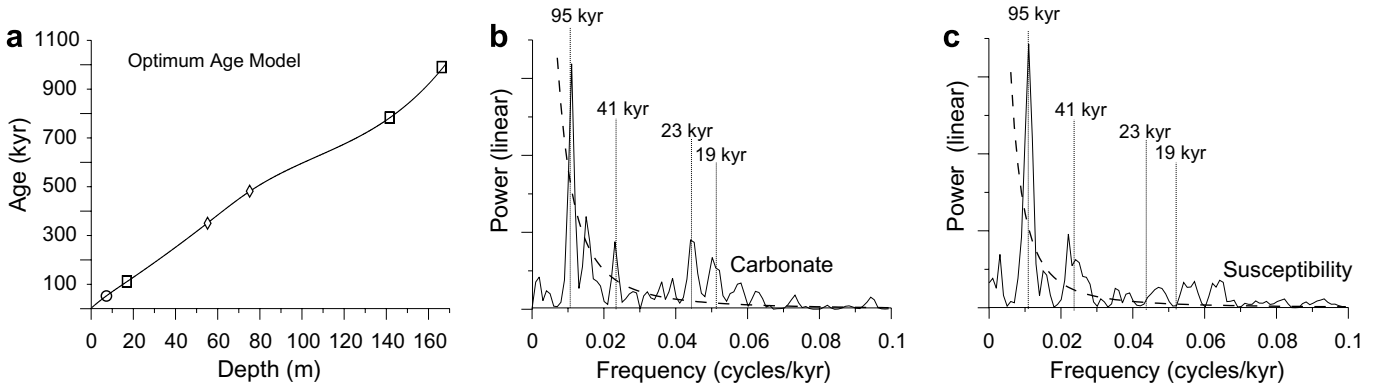


Fig. 7. (a) *Optimum age model* (full line) obtained by cubic spline interpolation using tie points from ^{14}C (circle), magnetostratigraphy (squares), and wavelength analysis (diamonds). The following tie points were included: 7.3 m/51.6 ka (^{14}C), 17.0 m/115 ka (Blake Event), 55.0 m/350 ka (wavelength analysis), 75.0 m/480ka (wavelength analysis), 141.5 m/780 ka (B/M boundary), 167.0 m/990 ka (upper Jaramillo boundary). Fourier spectra of whole-core carbonate (b) and susceptibility (c) time series using the optimum age model; significance level is shown by dashed lines.

curve is calculated using the ^{14}C date and assuming a constant rate of deposition for depths between 8.5 and 26.7 m. In this way, a *bandpass age model* is derived with linear and cubic spline interpolations (using cubic spline functions of the MATLAB toolbox) (Fig. 6b). Whole-core spectral analysis was carried out for carbonate data using both, the cubic spline (Fig. 6c) and linear model (not shown). Both spectra show low power for the obliquity cycle and a distortion of precession cycles. It has to be mentioned that a similar approach with higher resolution, using obliquity and precession cycles, is not feasible as counting of peaks is very ambiguous in the respective filtered curves (Fig. 6a).

Carbonate curves can be tentatively correlated to the marine oxygen isotope record (Fig. 3c), however, such correlations have large uncertainties. Attempts to derive a convincing age model failed. None of the possible correlations delivered a Fourier spectrum showing a complete Milankovitch band.

An *optimum age model* is established by cubic spline interpolation based on tie points from wavelength analysis (using sedimentation rates of 15 cm/kyr for 0–65 m, and 19 cm /kyr for 65–168 m), radiocarbon dating and magnetic ages ('true' ages of Blake Event, B/M boundary, upper Jaramillo boundary) (Fig. 7a). Whole-core spectral results of both, carbonate (Fig. 7b) and susceptibility (Fig. 7c) clearly show the eccentricity peak (95 kyr), and also obliquity (41 kyr). The precession cycles (23 and 19 kyr) are well indicated for carbonate but not for susceptibility. Reduced significance of precession in the susceptibility variations could be due to more regional influences. The improved spectrum of carbonate indicates that our interpretation of Jaramillo is justified. The complete depth-to-time conversion of the optimum age model is given in detail in Appendix A.

5. Conclusions

The *optimum age model* represents a best transformation of depth-to-time for the Heqing core. Accordingly the Heqing core spans almost the complete past 1 Myr (5–1001 ka). Calibrated ages (Appendix A) provide the essential basis for high-resolution dating of the existing (Yang et al., 2000; Hu et al., 2005) and future palaeoclimatic results from the Heqing core. The complete Milankovitch band observed in the carbonate data indicates that a global palaeoclimatic signal is recorded throughout most of the sequence. It is worth to note that the remarkable change at 65 m (Hu et al., 2005) corresponds to MIS11 deglacial warming (Droxler et al., 1999; Howard, 1997).

Our approach to determine the optimum age model is based on an average signal of Milankovitch cyclicities instead of counting individual cycles which cannot be determined unambiguously. This approach may be a promising way for fine-tuning of age of other long-term lacustrine sequences.

Acknowledgements

This work was financially supported by the National Natural Science Foundation of China (49872058, 40374021, 40172102) and the Deutsche Forschungsgemeinschaft (AP 34/15). The first author thanks for the financial support from the Department of Geology, University of California (Davis). We thank X. Jiang, H. Li, and C. Berthold for magnetic susceptibility, carbonate, and XRD measurements, respectively. We also thank R. Wu, Z. Zhang, W. Xia, and B. Xue for their contribution in fieldwork. Comments of G. Muttoni helped to improve the manuscript.

Appendix A

Depth-to-time conversion according to the *optimum age model*

Depth (m)	Age (ka)	Depth (m)	Age (ka)	Depth (m)	Age (ka)	Depth (m)	Age (ka)
0.25	4.00	46.00	290.34	92.00	563.82	138.00	761.40
1.00	9.66	47.00	296.87	93.00	568.06	139.00	767.11
2.00	17.01	48.00	303.43	94.00	572.24	140.00	772.95
3.00	24.15	49.00	310.01	95.00	576.38	141.00	778.91
4.00	31.10	50.00	316.61	96.00	580.47	142.00	785.00
5.00	37.88	51.00	323.24	97.00	584.52	143.00	791.22
6.00	44.49	52.00	329.89	98.00	588.54	144.00	797.58
7.00	50.96	53.00	336.57	99.00	592.51	145.00	804.07
8.00	57.30	54.00	343.27	100.00	596.46	146.00	810.71
9.00	63.52	55.00	350.00	101.00	600.38	147.00	817.50
10.00	69.65	56.00	356.75	102.00	604.28	148.00	824.44
11.00	75.69	57.00	363.52	103.00	608.16	149.00	831.53
12.00	81.66	58.00	370.29	104.00	612.03	150.00	838.79
13.00	87.58	59.00	377.07	105.00	615.88	151.00	846.20
14.00	93.45	60.00	383.85	106.00	619.73	152.00	853.78
15.00	99.30	61.00	390.61	107.00	623.57	153.00	861.53
16.00	105.15	62.00	397.36	108.00	627.41	154.00	869.46
17.00	111.00	63.00	404.08	109.00	631.26	155.00	877.56
18.00	116.87	64.00	410.76	110.00	635.11	156.00	885.84
19.00	122.76	65.00	417.41	111.00	638.98	157.00	894.31
20.00	128.67	66.00	424.00	112.00	642.85	158.00	902.97
21.00	134.61	67.00	430.54	113.00	646.75	159.00	911.82
22.00	140.57	68.00	437.02	114.00	650.67	160.00	920.86
23.00	146.55	69.00	443.43	115.00	654.62	161.00	930.11
24.00	152.55	70.00	449.76	116.00	658.60	162.00	939.56
25.00	158.57	71.00	456.01	117.00	662.61	163.00	949.22
26.00	164.62	72.00	462.16	118.00	666.66	164.00	959.09
27.00	170.69	73.00	468.22	119.00	670.75	165.00	969.17
28.00	176.78	74.00	474.16	120.00	674.89	166.00	979.47
29.00	182.89	75.00	480.00	121.00	679.08	167.00	990.00
30.00	189.03	76.00	485.72	122.00	683.31	168.00	1000.75
31.00	195.19	77.00	491.32	123.00	687.61		
32.00	201.37	78.00	496.80	124.00	691.96		
33.00	207.57	79.00	502.18	125.00	696.38		
34.00	213.80	80.00	507.45	126.00	700.87		
35.00	220.05	81.00	512.62	127.00	705.43		
36.00	226.32	82.00	517.69	128.00	710.07		
37.00	232.62	83.00	522.66	129.00	714.78		
38.00	238.94	84.00	527.55	130.00	719.58		
39.00	245.28	85.00	532.35	131.00	724.46		
40.00	251.65	86.00	537.06	132.00	729.44		
41.00	258.04	87.00	541.70	133.00	734.51		
42.00	264.45	88.00	546.26	134.00	739.67		
43.00	270.89	89.00	550.75	135.00	744.94		
44.00	277.35	90.00	555.17	136.00	750.32		
45.00	283.83	91.00	559.52	137.00	755.80		

References

Bleil, U., Gard, G., 1989. Chronology and correlation of quarternary magnetostratigraphy and nanofossil biostratigraphy in Norwegian-Greenland Sea sediments. Geology Rundschau 78, 1173–1187.

Burbank, D.W., Johnson, G.D., 1982. Intermontane basin development in the past 4 Myr in the north-west Himalaya. Nature 298, 432–436.

Cande, S.C., Kent, D.V., 1995. Revised calibration of the geomagnetic polarity timescale for the late Cretaceous and Cenozoic. Journal of Geophysical Research 100, 6093–6095.

Channell, J.E.T., Raymo, M.E., 2003. Paleomagnetic record at ODP Site 980 (Feni Drift, Rockall) for the past 1.2 Myrs. Geochemistry, Geophysics, Geosystems 4, 1–14.

Droxler, A.W., Poor, R., Burckle, L., 1999. Data on past climate warmth may lead to better model of warm future. EOS Transactions 80, 289–290.

Herbert, T.D., 1992. Paleomagnetic calibration of Milankovitch cyclicity in lower cretaceous sediments. Earth Planetary Science Letters 112, 15–28.

Hoffmann, V., 1992. Greigite (Fe_2S_4). Magnetic properties and first domain observations. Physics of the Earth and Planetary Interiors 70, 288–301.

House, M.R., 1985. A new approach to an absolute time scale from measurements of orbital cycles and sedimentary microrhythms. Nature 315, 721–725.

Howard, W.R., 1997. A warm future in the past. Nature 388, 418–419.

Hu, S., Wang, S., Appel, E., 1998. Remanence acquisition and alteration in lake sediments. Chinese Science Bulletin 43 (17), 1421–1434.

Hu, S., Goddu, S.R., Appel, E., Verosub, K., Yang, X., Wang, S., 2005. Palaeoclimatic changes over the past 1 million years derived from lacustrine sediments of Heqing basin (Yunnan, China). Quaternary International 136, 123–129.

Kukla, G., Clerk, V., 1996. Plio-Pleistocene megacycles: record of climate and tectonics. Palaeogeography, Palaeoclimate and Palaeoecology 120, 171–194.

Kukla, G., Heller, F., Liu, X.M., Xu, T.C., Liu, T.S., An, Z.S., 1988. Pleistocene climates in China dated by magnetic susceptibility. Geology 16, 811–814.

Mayer, H., Appel, E., 1999. Milankovitch cyclicity and rock-magnetic signatures of palaeoclimatic change in the Early Cretaceous Biancone Formation of Southern Alps, Italy. Cretaceous Research 20, 189–214.

Ruddiman, W.F., Raymon, M., McIntyre, A., 1986. Matuyama 41,000 year cycles; North Atlantic ocean and northern hemisphere ice sheets. Earth Planetary Science Letters 80, 117–128.

Schulz, M., Stattegger, K., 1997. SPECTRUM : Spectral analysis of unevenly spaced palaeoclimatic time series. Computers and Geosciences 23, 929–945.

Schulz, M., Mudelsee, M., 2002. REDFIT: estimating red-noise spectra directly from unevenly spaced paleoclimatic time series. Computers and Geosciences 28, 421–426.

Schwarzacher, W., 1993. Cyclostratigraphy and the Milankovitch Theory. Developments in Sedimentology 52, 225.

Singer, B., Brown, L.L., 2002. The Santa Rosa Event; 40Ar/39Ar and paleomagnetic results from the Valles rhyolite near Jaramillo Creek, Jemez Mountains, New Mexico. Earth and Planetary Science Letters 197, 51–64.

Thouveny, N., De Beaulieur, J., Bonifay, E., Creer, K.M., Gulot, J., Icole, M., Johnson, S., Jouzel, J., Reille, M., Williams, T., Williamson, D., 1994. Climate variations in Europe over the past 140 kyr deduced from rock magnetism. Nature 371, 503–506.

Verosub, K.L., Banerjee, S.K., 1977. Geomagnetic excursion and their paleomagnetic record. Reviews of Geophysics and Space Physics 15, 145–155.

Wang, S.M., Hu, S., Appel, E., Ma, X.H., Hoffmann, V., Sun, Z.M., Yang, X.D., Ma, Y., Pan, H.X., 1999. Incursion of sea water into Gucheng lake detected by magnetic, biologic and chemical data. Physics and Chemsitry of the Earth 24, 805–809.

Williams, D.F., Peck, J., Karabanov, E.B., Prokopenko, A.A., Kravchinsky, V., King, J., Kuzmin, M.I., 1997. Lake Baikal record of continental climate response to orbital onsolation during the past 5 million years. Science 278, 1114–1117.

Yang, X., Wang, S., Tog, G., Jiang, X., 2000. Vegetational and climatic responses to tectonic uplift in the Heqin Basin of Yunnan Province during the past 1.0 Ma. Acta Micropaleontologica Sinica 17, 207–217.

Yang, T.S., Hyodo, M., Yang, Z.Y., Fu, J.L., 2004. Evidence for the Kamikatsura and Santa Rosa excursions recorded in eolian deposits from southern Chinese Loess Plateau. Journal of Geophysical Research 109, B12015.